Effects of direction reversals on patterns of active filaments

Leila Abbaspour[1,2,3,*] Ali Malek,[2] Stefan Karpitschka,[3] and Stefan Klumpp[1,2,†]

[1]*Max Planck School Matter to Life, University of Göttingen, Friedrich-Hund-Platz 1, 37077 Göttingen, Germany*

[2]*Institute for the Dynamics of Complex Systems, University of Göttingen, Friedrich-Hund-Platz 1, 37077 Göttingen, Germany*

[3]*Max Planck Institute for Dynamics and Self-Organization, Am Faßberg 17, 37077 Göttingen, Germany*

(Received 16 November 2022; accepted 10 February 2023; published 13 March 2023)

Active matter systems provide fascinating examples of pattern formation and collective motility without counterpart in equilibrium systems. Here, we employ Brownian dynamics simulations to study the collective motion and self-organization in systems of self-propelled semiflexible filaments, inspired by the gliding motility of filamentous *Cyanobacteria*. Specifically, we investigate the influence of stochastic direction reversals on the patterns. We explore pattern formation and dynamics by modulating three relevant physical parameters, the bending stiffness, the activity, and the reversal rate. In the absence of reversals, our results show rich dynamical behavior including spiral formation and collective motion of aligned clusters of various sizes, depending on the bending stiffness and self-propulsion force. The presence of reversals diminishes spiral formation and reduces the sizes of clusters or suppresses clustering entirely. This homogenizing effect of direction reversals can be understood as reversals providing an additional mechanism to either unwind spirals or to resolve clusters.

DOI: 10.1103/PhysRevResearch.5.013171

I. INTRODUCTION

Active matter is a class of systems that are inherently out of equilibrium through coupling to an internal process of energy consumption that results, for example, in self-propulsion or growth [1,2]. Specifically, the case of self-propelled active particles has received much attention in recent years, as it gives rise to intriguing dynamics and mechanical behavior at the collective level. Such systems are ubiquitous in nature, examples include the cytoskeleton [3–5], swarming bacteria [6–8], tissues [9], and biofilms [10]. Finding suitable tools to study active matter systems is a challenge for nonequilibrium statistical physics in order to elucidate the dynamical behavior and the physical properties of these systems.

Self-propelled particles self-organize into macroscopic structures with collective dynamics like clustering, swarming, and swirling. This type of dynamical pattern formation has been subject to intensive research in recent years, both from a theoretical or computational viewpoint [11–25] and experimentally [26–34], often using systems of bacteria either swimming in a solution or gliding on surfaces as well as synthetic self-propelled particles systems [35,36].

On the theoretical side, most studies of collective effects in systems of self-propelled particles have considered either spherical or point-like particles or short and rigid rod-like particles, as these are good approximations for the shape of the bacteria typically used in experiments such as swimming *Bacillus subtilis* or *Escherichia coli* [13,23,32] and as *Myxococcus xanthus*, gliding on surfaces [28]. The aspect ratio of rod-like particles has a strong impact on the patterns, as high aspect ratios promote (nematic) alignment of the particles and swarming [37].

At very large aspect ratios, the finite bending rigidity of the particles is expected to play a role. Therefore several recent computational studies have addressed semiflexible filamentous particles or self-propelled polymers [14,15,38]. Indeed, their collective behavior is modulated by their bending rigidity. Moreover, flexibility even results in new single-filament behavior, as individual flexible filaments are seen to curl into spirals due to their self-propulsion [21].

Complicating the understanding of the behavior of the collective motion of microbes, many of them, in addition to active self-propulsion, also perform active directional changes such as the well-known run-and-tumble motion of *Escherichia coli* [39]. Typically, these active direction changes are an integral part of the mechanisms for chemotaxis and other types of tactic behaviors, through a coupling of the rates of directional change to the direction of motion relative to a (chemical, light, etc.) gradient direction. Such active directional changes have occasionally been included in models for the motility and collective behavior of self-propelled particles [18,40–44] or spreading of active polymers in porous media [45]. For bacteria, the simplest direction change is a reversal, where the whole filament reverses its direction of motion by 180°, as seen in the gliding motility of *M. xanthus*, a short rigid rod [28], as well as in gliding filamentous *Cyanobacteria* [46,47].

In this article, we use agent-based simulations to address how such reversals affect the collective behaviors of self-propelled semiflexible filaments at overall relatively low density. To that end, we first consider the reference case without reversals and analyze the formation of spirals and

*leila.abbaspour@mtl.maxplanckschools.de

†stefan.klumpp@phys.uni-goettingen.de

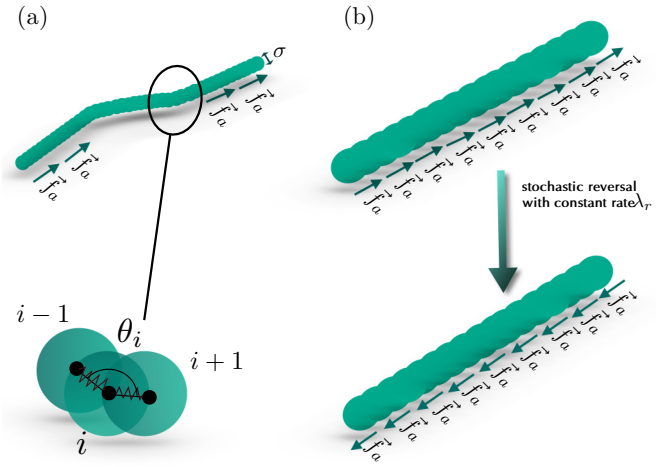

FIG. 1. Model of a self-propelled filament. (a) Sketch of a self-propelled filament composed of monomers with diameter σ. The active force inducing their self-propulsion acts tangentially along each bond. (Zoom) The flexibility of the chain is modeled by a harmonic bending potential, where θ_i is the angle formed by each successive triplet of monomers $i-1, i, i+1$. (b) Sketch of the reversal mechanism of a self-propelled filament. Upon a stochastic reversal with rate λ, a filament reverses the direction of its self-propulsion force by 180°.

swarms or clusters. Then we turn to the case with stochastic direction reversals, generated by a Poisson process, and investigate their impact on these patterns.

We focus on the interplay of the filaments' self-propulsion force, bending stiffness, and reversal rate as the control parameters that modulate the pattern formation process. In the absence of reversals, the filaments form spirals for high self-propulsion force and low bending stiffness, for larger bending stiffness coherently moving clusters dominate the system. Introducing reversals reduces the rates of forming either type of pattern, and thus the system becomes gradually more isotropic with increasing reversal rate. The suppression of either pattern can be explained by the dynamical pathway of these structures: First, reversals add a mechanism that interrupts the spooling of a filament onto itself and initiates unwinding. Second, similarly, reversals allow filaments to leave a cluster as they break the coherence of motion in clusters.

II. MODEL

A. Self-propelled filaments

We consider a system of N_c self-propelled semiflexible filaments. The individual filament is described as a chain of N monomers located at positions $(\vec{r}_1, \vec{r}_2, \cdots, \vec{r}_N)$ in space [see Fig. 1(a) for a schematic]. Two consecutive monomers in the chain are connected by a harmonic spring. In addition, the angle between three consecutive monomers along the chain are subject to a harmonic bending potential, which controls the flexibility of the chain. In the overdamped regime, the equation of motion for each monomer can be written as

$$\zeta \dot{\vec{r}}_i = -\nabla_i U_s - \nabla_i U_b + \vec{F}_i^a + \vec{F}_i^{ex} + \vec{F}^{\text{rand}}. \tag{1}$$

where $\dot{\vec{r}}_i$ is the velocity of the ith monomer, ζ is the friction coefficient. The five force contributions on the right-hand side of this equation represent stretching and bending of the chain, the active force responsible for self-propulsion, volume exclusion, and stochastic noise, respectively.

U_s is the stretching potential due to the harmonic springs (each with an equilibrium length of r_0 between consecutive monomers) with the form

$$U_s = \frac{\kappa_s}{2} \sum_{j=2}^{N} (r_{j,j-1} - r_0)^2. \tag{2}$$

where $r_{j,j-1} = |\vec{r}_j - \vec{r}_{j-1}|$ is the distance between the jth and $j-1$th monomer and κ_s is the spring constant associated with stretching.

U_b is the harmonic bending potential, which controls the flexibility of the bonds. Considering θ_i as the angle formed by a consecutive triplet of monomers $(i-1, i, i+1)$, given by $\theta_i = cos^{-1}(\frac{\vec{r}_{i-1,i} \cdot \vec{r}_{i,i+1}}{|\vec{r}_{i-1,i}||\vec{r}_{i,i+1}|})$, this potential is defined as

$$U_b = \frac{\kappa_b}{2} \sum_{j=2}^{N-1} (\theta_j - \pi)^2, \tag{3}$$

where π is the equilibrium angle of between adjacent pairs of monomers, corresponding to a straight chain, and κ_b is the spring constant associated with bending.

The self-propulsion is induced by the active force $\vec{F}_i^a$,

$$\vec{F}_i^a = f_a \hat{t}_i, \tag{4}$$

where f_a fixes the absolute value of the self-propulsion force and $\hat{t}_i$, the unit vector tangent to the chain at the position of ith monomer, defines its direction. For a chain consisting of discrete monomers, this vector can be approximated as

$$\hat{t}_i = \frac{\alpha_c}{2} \left(\frac{\vec{r}_{i+1,i}}{|\vec{r}_{i+1,i}|} + \frac{\vec{r}_{i,i-1}}{|\vec{r}_{i,i-1}|} \right). \tag{5}$$

Here $\alpha_c \in \{-1, +1\}$ specifies the state of the polarity (head-tail) for each chain $c \in \{1, \cdots, N_c\}$ where N_c is the number of chains in the system. This variable will be important for the modeling of reversal events, as we will discuss below.

The presence of the repulsive force $\vec{F}_i^{ex}$ prevents overlaps of the monomers. Such volume exclusion is implemented using the Week-Chandler-Anderson potential,

$$U_{ext}(r) = \begin{cases} 4\epsilon\left[\left(\frac{\sigma}{r}\right)^{12} - \left(\frac{\sigma}{r}\right)^{6}\right] + \epsilon, & r < 2^{1/6}\sigma \\ 0, & \text{otherwise} \end{cases} \tag{6}$$

where σ is the nominal interaction diameter and ϵ is the energy scale of the interaction. As an exception from volume exclusion, adjacent monomers in the filament are taken to overlap with distance $r_0 = \sigma/2$, in order to obtain a smooth filament.

The stochastic term F_{rand} represents thermal fluctuations and is given by white noise. In the simulations that we report in the following, we neglect this term, because it is very small compared to the deterministic contributions. In particular, motion of the filaments is dominated by self-propulsion and bending of the filaments is induced by collisions between filaments. For convenience, we will, nevertheless, use the thermal energy, $k_B T$ to set the energy scale with $T = 300\,\text{K}$.

B. Direction reversals

So far, our model agrees with previous models for self-propelled filaments [14,15,21]. In addition, we include spontaneous reversals of the direction of self-propulsion, as they are often seen in the surface motion of bacteria [45,48] including filamentous species such as gliding filamentous *Cyanobacteria* [47,49,50]. Typically, the rates for such reversals are modulated by various tactic behaviors such as chemotaxis, phototaxis, etc. Here we consider the baseline case of spontaneous reversals in a homogeneous environment.

We model random reversal events, where the gliding direction of a chain changes instantaneously by 180°, as generated from a Poisson process with a reversal rate λ_r [see Fig. 1(b)]. Mathematically, this means that the polarity (head-tail) state α_c of a chain c follows a stochastic process

$$\alpha_c = 1 \quad \underset{\lambda_r}{\overset{\lambda_r}{\rightleftharpoons}} \quad \alpha_c = -1. \tag{7}$$

In such a Poisson process, the distribution of waiting times τ elapsed between two consecutive reversals is an exponential distribution of the form

$$P_{\rm w}(\tau) = \lambda_r e^{-\lambda_r \tau}. \tag{8}$$

There is experimental evidence for exponential waiting time distributions between reversals or other active direction changes in swimming bacteria [51,52]. For gliding bacteria on surfaces, which provide examples for active filaments, this is less clear, so we use an exponential distribution, i.e., a constant rate for reversals, as the simplest possible choice. To implement the reversals for a single chain, we draw a random waiting time τ_0 from the exponential distribution described in Eq. (8) at time t_0. Between t_0 and $t_1 = t_0 + \tau_0$, the chain evolves following Eq. (1). At t_1 the gliding direction of the chain is reversed and another waiting time τ_1 is drawn from the same waiting time distribution. This process is done for each chain independently during the simulation by drawing subsequent time intervals τ_2, τ_3, ..., such that reversals of any chain in the system is uncorrelated with the reversal of any other chains. Given a reversal rate λ_r and a free propulsion speed of f_a/ζ, the free propagation distance between reversals on average is $L_r = f_a/(\zeta\,\lambda_r)$.

C. Simulations and parameters

All simulations presented here were run on GPUs using the simulation package HOOMD-blue [53] with custom extensions for self-propulsion and for reversals, which were compiled together with the whole software. The simulations integrate Eq. (1) over $t = 10^8$ time steps with periodic boundary conditions and we take 200 snapshots in the last quarter of the simulation time for each condition over which ensemble averages are taken. For some result we averaged in addition over five independent simulation runs.

To initialize the system, we place N_c semiflexible filaments on a grid with a folded structure of the chain and then randomly rotate each filament around its own center of mass to give them a random orientation. We then integrate the equations of motion for a few thousand time steps with an additional random force to obtain a fully isotropic configuration, which is used as the initial configuration of our simulation.

In these simulations, lengths are measured in units of the monomer diameter σ and the energy unit is k_BT. We choose the time unit to be the self-diffusion time for a single monomer $\tau_D = \frac{\sigma^2\zeta_0}{k_BT}$ with the arbitrary reference friction coefficient ζ_0. In the simulations, we use a friction coefficient $\zeta = 15\zeta_0$. The reversal rates are thus given in units of τ_D^{-1}.

Our system consists of $N_f = 1666$ filaments each having $N_m = 59$ monomers. This choice sets the aspect ratio, a dimensionless number representing the ratio between the contour length and the diameter of the individual monomers $a = \frac{L_f}{\sigma}$, to 30. Here $L_f = (N_m + 1)r_0$ is the contour length of the filaments. We set the spring constant of the stretching spring to $\kappa_s = 10^4$, i.e., to a relatively high value to make sure that chains do not stretch too much along their axis. Hence the distance between two successive monomers does not fluctuate strongly and is approximately constrained to the fixed value r_0. Furthermore, to obtain a smoother filament, we also set the value $r_0 = \frac{\sigma}{2}$. To investigate a large parameter space, we varied κ_b in the range $\{1, 1800\}$ and f_a between $\{1, 100\}$. The packing fraction $\phi = N_f N_m r_0 \sigma / L^2$ is set to 0.1 in all simulations, where L denotes the box size and $L = 167\sigma$ (this choice determines the number of filaments to $N_f = 1666$ as mentioned above). The reversal rates λ_r are varied between $\{0 - 0.1\}$ and are the same for all the filaments.

III. RESULTS

To address the effect of direction reversals on the collective dynamics of self-propelled filament, we performed systematic simulations varying three key parameters, the bending stiffness κ_b, the strength of self-propulsion f_a, and the reversal rate λ_r. We will show typical snapshots of these simulations below. We start with the case without direction reversals ($\lambda_r = 0$), which has been studied before [14,15] and which serves us as a reference scenario here. In that case, it is known that a variety of nonequilibrium patterns can be formed, for which we will present a detailed diagram of states below.

Later on, we add the reversal mechanism to the filaments, inspired by the reversal dynamics observed in filamentous *Cyanobacteria* to investigate the response of the system to an abrupt and random reversal in gliding direction. We report a dramatic change in the individual as well as collective dynamics in the state diagram as we crank up the reversal rate, eventually destroying the spiral state completely and leading to destruction of clusters and collective motion.

A. Nonreversing active filaments

1. Spiral formation

In the absence of direction reversals, the collective dynamics of the chains is dominated by the interplay between self-propulsion, bending stiffness and confinements due to the excluded volume effect. A key observation at low density of filaments is that flexible filaments may form spirals while stiffer filaments tend to form clusters [14,15].

Spirals form due to the self-interaction of an isolated active filament with high self-propulsion and low bending stiffness. Spiral formation stands in contrast to the relatively straight equilibrium structure of a semiflexible filament and depends on the self-propulsion. Spiral formation is initiated when the

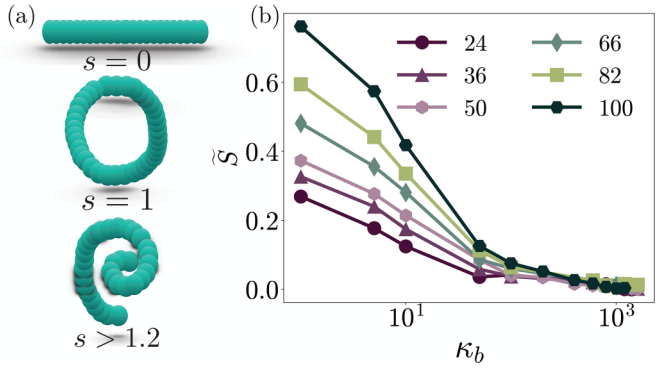

FIG. 2. Spiral ratio as a function of bending stiffness for different values of self-propulsion force. (a) Sketch of different configuration of a single filament characterised by the indicated spiral number indicated by s. (b) Quantification of spiral formation by the spiral ratio $\widetilde{S}$, the ratio of the number of filaments in the spiral state (with $s \geqslant 1.2$) to the number of filaments in the straight state (with $s < 1.2$): An increase in bending stiffness decreases the probability of spiral formation at a constant self-propulsion force. Different values for self-propulsion are shown in different colors. With increasing self-propulsion force at low bending stiffness, spiral formation is promoted. For high bending stiffness, spiral formation does not take place regardless of the self-propulsion force.

head of the filament collides with a subsequent part of its own body, such that the excluded volume interaction forces the filament to wind into itself. If the self-propulsion is strong enough, filaments get trapped in their own body, forming stable spirals. To characterise the dynamical state with spiral formation we define a spiral number [21] for each filament in the system, which quantifies how many times a filament is wound up around itself and is defined as

$$s = \left| \frac{\sum_{i=2}^{N-2} \Delta\theta_i}{2\pi} \right| \tag{9}$$

where θ_i is the angle formed by the beads $i-1, i, i+1$. $|..|$ denotes the absolute value of the spiral number since they can be twisted either in the clockwise or counterclockwise direction. $s = 0$ indicates an almost straight configuration [see Fig. 2(a)] and $s = 1$ a ring shape [see Fig. 2(a)]. We consider a filament to be in a spiral state if $s \geqslant 1.2$ [see Fig. 2(a)].

To distinguish global patterns of filaments, we introduce the spiral ratio as the ratio of the number of filaments in the spiral state (i.e., with $s \geqslant 1.2$) N_s to that in the straight configuration N_{sf},

$$\widetilde{S} = \frac{N_s}{N_{sf}}. \tag{10}$$

The spiral ratio is plotted in Fig. 2(b) as a function of the bending stiffness and the self-propulsion force. The figure shows a pronounced decrease of the spiral ratio with increasing bending stiffness, which reflects the fact that increasing bending stiffness (κ_b) hinders the self-interaction needed for spiral formation. Figure 2(b) also shows that, for fixed bending rigidity, spiral formation is promoted by an increase in the self-propulsion force.

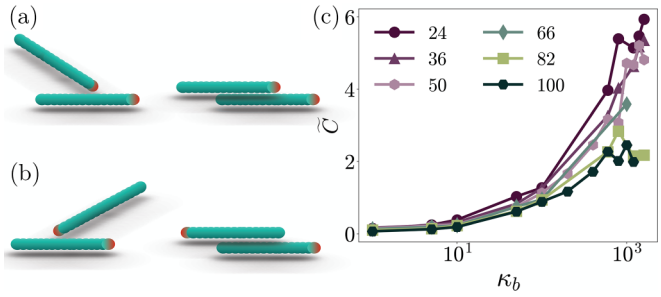

FIG. 3. Cluster ratio as a function of bending stiffness for different values of self-propulsion force. (a) A binary collision of self-propelled filaments that results in parallel alignment and coherent motion that initiates cluster formation. (b) A binary collision of self-propelled filaments that results in anti-parallel alignment and transient coherent motion. The red monomer shows the head of the filament in both cases. (c) Increasing the bending stiffness promotes cluster formation in the system, shown here by the cluster ratio, the ratio of the number of filaments in cluster to the number of filament that are not in clusters. Note that here we do not distinguish different categories of clusters by size. Different values for the self-propulsion force are shown in different colors.

2. *Cluster formation*

In the limit of high bending stiffness, filaments behave like rod-shaped agents. In this regime, filaments move in the direction of their long axis and, upon collisions, they rotate to align due to their steric interaction. At high bending stiffness, collisions between filaments are dominant over self-interactions as the bending energy required for the self-interaction is rarely reached. Dependent on the angle of incidence of the collision event, the two filaments align either parallel or antiparallel [Figs. 3(a) and 3(b), respectively]. In the first case, they continue their motion together, in the second case, they stay in contact transiently [1,18]. Clusters of filaments form when additional filaments collide with already aligned filaments, resulting in groups of filaments that move coherently. The size and life-time of these clusters depends on bending rigidity and activity, as well as the density of the filaments in the system [1,23,37].

To characterise the clustering behavior we identify clusters using the following criteria: two monomers are considered to be part of the same cluster if their centers are distanced less than 1.2σ. We note that this criterium automatically includes all monomers of one filament in the same cluster. In addition, we only considered clusters with at least $N_f = 10$ filaments to avoid counting micro clusters. Clusters are identified with the data analysis framework Freud [54]. Finally, in analogy to the spiral ratio, we define a cluster ratio as the ratio of number of filaments in clusters N_c to the number of free filaments N_f,

$$\widetilde{C} = \frac{N_c}{N_f}. \tag{11}$$

Figure 3 shows the cluster ratio as a function of the bending stiffness for different values of the active force. The cluster ratio is seen to increase monotonically with increasing bending stiffness (κ_b) and also with increasing self-propulsion force. One can also see that high values of the spiral number are associated with small clusters and vice versa: the regions with

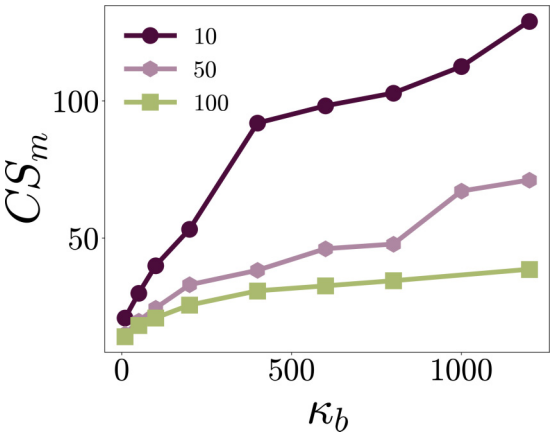

FIG. 4. Average cluster size as a function of bending stiffness. The average cluster size is shown in different colors for different self-propulsion forces. The data are averages over 1000 snapshots from five independent simulation runs in addition to averaging over 200 snapshots per run.

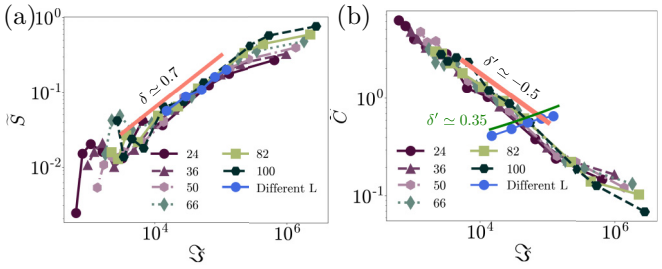

FIG. 5. (a) Spiral ratio $\widetilde{S}$ and (b) cluster ratio $\widetilde{C}$ as functions of the flexure number $\Im$. Data collapse for different self-propulsion forces and bending rigidities when these are plotted as functions of a dimensionless combination, the flexure number. The color of the points indicates the value of the self-propulsion force. The blue line with the circle marks shows results obtained by varying the filament length. The data points for different lengths fall onto the curve obtained by varying the bending stiffness and the self-propulsion force for the spiral ratio, but not for the cluster ratio. The red lines indicate power laws fitted to the curves, with exponents δ and δ'. The green line indicates power laws fitted to the cluster ratio curve for filaments of different lengths, with exponent δ' in green.

higher values of spiral ratio in Fig. 2 correspond to the region of low cluster ratio in Fig. 3. When the bending stiffness is low, spirals are formed due to the self-interaction, when the bending stiffness increases, the deformation of the filaments becomes unfavorable, which is why they usually have a straight, rod-like conformation that promotes alignment and, thus, clustering.

We also define the average cluster size CS_m, which is the average total number of filaments belonging to clusters and this seems to increase with increasing bending stiffness indicating (see Fig. 4) the fact that bending stiffness, which suppress spiral formation, promotes clustering.

Since both spiral ratio and cluster ratio show opposing trends as function of the bending rigidity and of the self-propulsion force, we wondered whether the results could be written as functions of a dimensionless parameter combination. A natural candidate is the flexure number, the ratio of activity and bending rigidity [14,15,55,56], which can be written as

$$\Im = \frac{f_a L^3}{\kappa_b}. \tag{12}$$

Figure 5 shows the spiral and cluster ratio as functions of the flexure number. Indeed the data from simulations with different bending stiffness and self-propulsion forces are seen to collapse onto one curve. Only for the largest flexure numbers, we see systematic deviations for the spiral ratio. For smaller values of the flexure number, the spiral ratio increase as a power law $\tilde{S} \sim \Im^{\delta}$ with $\delta \simeq 0.7$. Likewise, the decrease of the cluster ratio also follows a power law $\tilde{C} \sim \Im^{\delta'}$ with $\delta' \simeq -0.5$. $\tilde{S}$ is seen to deviate from the power law for large $\Im$. The origin of that deviation is not clear, but the appearance of these deviations coincides with the transition from the cluster to the melt phase, so we suspect a connection to that transition.

Previous simulation studies [14,15] has shown spirals only for sufficiently long filaments, while the dependence of the spiral ratio on the flexure number shown in Fig. 5 suggests that reduced length could be compensated by increasing the flexibility of the filaments. We therefore simulated filaments of different lengths and determined the spiral ratio and included the data point in the plot of spiral ratio as function of the flexure number. Indeed the data points for different length fall nicely onto the same curve as obtained by varying the bending stiffness and the self-propulsion force [Fig. 5(a)]. So in principle, even short filament should form spirals if they are sufficiently flexible. Spiral formation for short filaments will however be limited by the discrete nature of the filaments that are represented by chains of beads. By contrast, the cluster ratio [blue dotted line in Fig. 5(b)] shows a very different behavior, and varying the filament length leads to a different curve than varying the bending stiffness or the self-propelling force also follows a power law $\widetilde{C} \sim \Im^{\delta'}$ with $\delta' \simeq 0.35$. By contrast, the cluster ratio shows very different behavior. Varying the filament length results in a different curve than varying the bending stiffness or self-propulsion force [Fig. 5(b)], indicating a key role of filament length for clustering. Specifically we find an increase rather of the cluster ratio with increasing flexure number rather than a decrease. This increase can also be described by a power law, at least over the range that we have simulated, $\widetilde{C} \sim \Im^{\delta'}$ with $\delta' \simeq 0.35$.

3. State diagram

We performed systematic simulations varying the self-propulsion force f_a and the bending stiffness κ_b to explore the variety of patterns in the steady state of the system.

To distinguish different states of the system, we assign a state to all filaments in a snapshot via the following criteria: A filament is considered as a spiral if its spiral number is <1.2. The filament is taken to be in the cluster category if it is not a spiral and part of a cluster of $\geqslant 10$ filaments. Since this criterion does not capture the diversity of cluster patterns, we further subdivide the cluster state by the size of clusters and distinguish a small-cluster category for filaments in clusters with size $\geqslant 10$ and <100 and a large-cluster category for filaments in clusters with $\geqslant 100$ filaments. All other filaments are considered to be in the melt state.

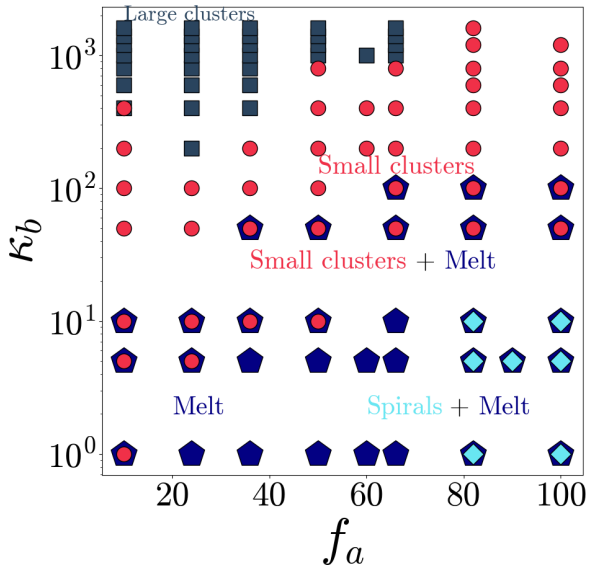

FIG. 6. Nonequilibrium state diagram of nonreversing self-propelled filaments. The state diagram is drawn as a function of self-propulsion force f_a and the bending stiffness κ_b in the absence of reversals. The different states are indicated by different symbols and the color of each symbol is matched to the corresponding designation of the state. For details on the characterisation and identification of the states, see text.

Using this classification and averaging over 200 snapshots per condition, we classify the state of the whole system into the following categories: A large-cluster state or a small-cluster state if $\geqslant$40% of the filaments are in large or small clusters, respectively. As the two criteria are not mutually exclusive, coexistence of small and large clusters is identified if both are satisfied simultaneously. Likewise, a spiral state is identified when more than 20% of the filaments form spirals (the threshold is chosen lower than for the other states, as under the conditions simulated here, we hardly ever see 40% of the filaments being spirals). Finally, the system state is classified as a melt state if $\geqslant$40% of the filaments fall into this category. Just like for small and large clusters, coexistence of other states is possible and indeed seen frequently, e.g., between melt and small clusters and melt and spirals. The diagram of states shown in Fig. 6 summarizes this classification. Simulation snapshots corresponding to the different states are shown in Fig. 7, where the color code of the filament shows the classification at the filament level.

For low bending stiffness and low self-propulsion force, the filaments are mostly in the melt (or isotropic) phase and move in all directions, as can be seen in Fig. 7(a). We note that while the melt filaments are dominant, there are also some small clusters. Increasing the self-propulsion force, while the bending stiffness is kept at a small value, promotes spiral formation, as shown in Figs. 7(b) and 7(c). Formation of spirals

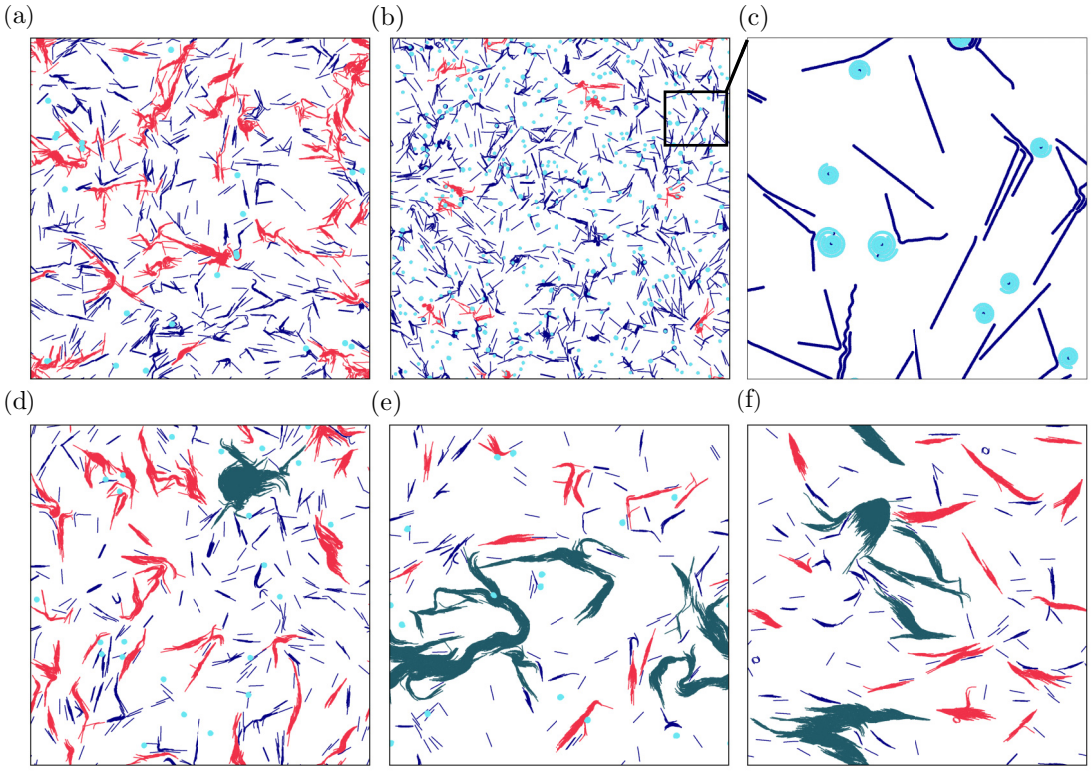

FIG. 7. Snapshots of the simulation for different f_a and κ_b. (a) Snapshot for $\kappa_b = 10$, $f_a = 10$ in "melt" state (b) $\kappa_b = 5$, $f_a = 100$ in spiral + melt state (c) Close-up view of spirals in plot (b). (d) $\kappa_b = 600$, $f_a = 82$ in small-cluster state. (e) $\kappa_b = 1000$, $f_a = 24$ in large-cluster state. (f) $\kappa_b = 1600$, $f_a = 10$ in large + small cluster state. The coloring of the filaments indicates their classification as spirals (cyan), filaments in small clusters (red), large clusters (gray-green), and a melt (blue).

is quite natural in this regime because the filaments are flexible enough to bend onto themselves. Their self-propulsion then results in spiral formation and, once formed, a spiral is typically stable until another filament collides with it.

Collisions with other filament seems to be the dominant (if not only) mechanism that breaks up spirals, since we have not included explicit translational or rotational noise in our simulations. Under the conditions we simulated, the spiral state typically coexists with the melt phase, as can be seen in the snapshots in Figs. 7(b) and 7(c). Consistent with this observation, a pure spiral state, the "gas of spirals" reported in earlier studies [15] is only observed at even lower densities than used here.

As shown above (Fig. 2), the fraction of spirals decreases with increasing bending rigidity. For sufficiently large bending stiffnesses, collective behavior via the formation of clusters becomes dominant over individual filament dynamics. In this regime, the self-interaction is less important compared to inter-filament interaction, and when filaments collide, they can bundle into small clusters with local alignment (nematic order). Over time, the clusters grow as other filaments collide with them and join them. At intermediate bending stiffness, there is a coexistence of dispersed individual filaments and small clusters [Fig. 7(d)]. As we increase the bending stiffness [Figs. 6(d)–6(f)], the clusters become larger and the system enters a large-cluster state, in particular for low self-propulsion force.

These observations show that the collective behavior of filaments is modulated by their bending stiffness and their self-propulsion force. In agreement with earlier studies [14,15], we distinguish several regimes, characterized by the formation of spirals and of clusters of various sizes. Generally, we observed that, in the absence of direction reversals, filaments with high self-propulsion force and low bending stiffness form spirals, while filaments with high bending stiffness tend to form clusters. This general picture will serve as a reference in the following section, where we will include direction reversals and study how the variation of the reversal rate affects the patterns formed by self-propelled filaments.

B. Active filaments with direction reversals

Next, we consider active filaments that exhibit reversals of their direction of motion. Many microorganisms exhibit such a feature in their motility (both swimming and surface-bound species), often as part of their chemo- or phototactic strategy. Here we consider the case of spontaneous, nonbiased stochastic reversals. Our filaments are taken to change their direction of motion abruptly, by 180°, according to a Poisson process with rate λ_r. Varying λ_r, we explored the effect of reversals on the structures and the collective motion of the active filaments.

Figure 8 demonstrates the effect of a small reversal rate $\lambda_r = 0.1$ (right column) compared to the case without reversals (left column) for two opposite corners of the state diagram Fig. 6. These two parameters sets chosen here correspond to the regime exhibiting spirals ($f_a = 100$ and $\kappa_b = 1$, top) and to the regime dominated by small clusters ($f_a = 24$ and $\kappa_b = 1000$, bottom). In both cases, the visual appearance of patterns clearly changes, indicating a substantial influence of the reversals. In the spiral + melt regime (large f_a and small κ_b), spirals (light blue) are abundant (though in coexistence with straight filaments) in absence of reversals, but efficiently suppressed by a small reversal rate $\lambda_r = 0.1$. In the large-cluster regime (small f_a and large κ_b), the change is less dramatic as collectively moving clusters are seen both with and without reversals. However, the size of the clusters is considerably decreased by the reversals.

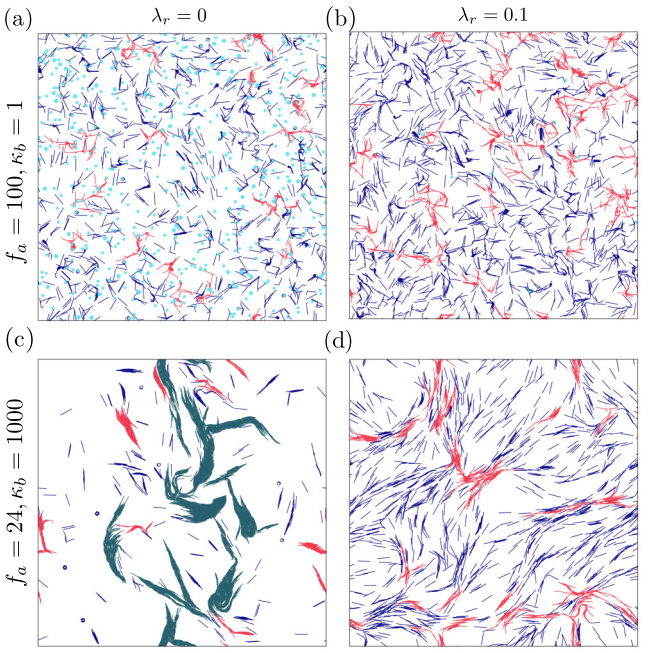

FIG. 8. Snapshot of the simulation with reversal dynamics. We show snapshots from the simulations keeping the bending stiffness, activity, density, and aspect ratio same and changing the reversal rate. Applying reversal rate changes the pattern formation drastically from its nonreversing counterpart. [(a),(b)] In the presence of a nonzero reversal rate, spiral formation has disappeared. [(c),(d)] Likewise, in the presence of reversals, the cluster sizes become smaller than the nonreversing case. The coloring of the filaments indicates their classification as spirals (cyan), filaments in small clusters (red), large clusters (gray-green), and a melt (blue).

1. Unwinding and declustering

To quantify the weakening of spiral and cluster formation, we determined again the spiral and cluster ratio, for a large range of reversal rates λ_r, for an intermediate value of f_a=50.

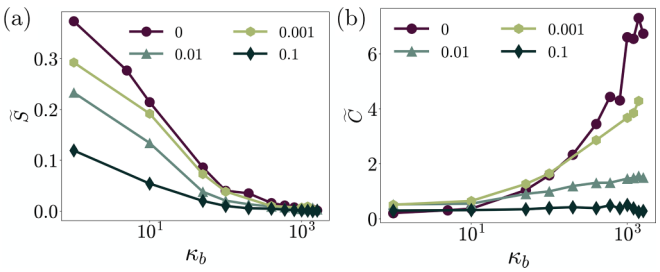

FIG. 9. (a) Spiral ratio ($\widetilde{S}$) and (b) cluster ratio ($\widetilde{C}$) for different reversal rates λ_r is shown in different colors at an active force, $f_a = 50$.

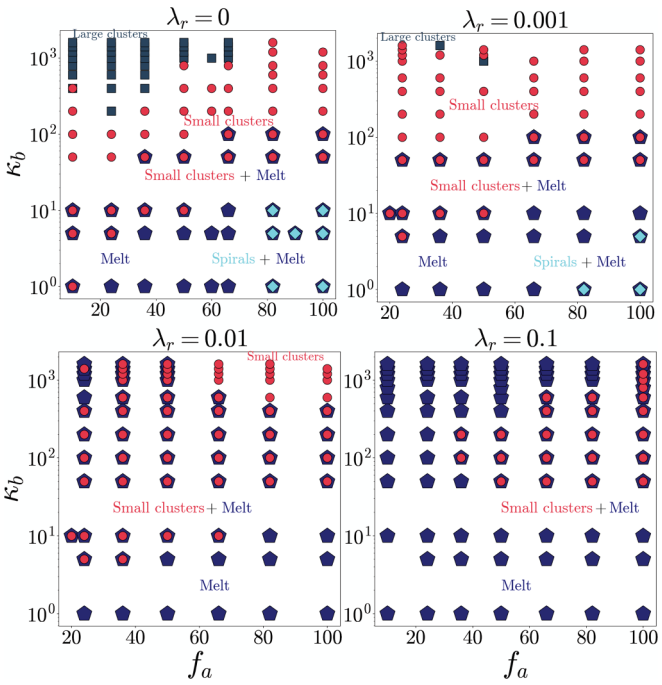

FIG. 10. Diagram of state for reversing self-propelled filaments. The state diagram is constructed as a function of the self-propulsion force f_a and the bending stiffness κ_b and shown for four different values of the reversal rate λ_r. States are marked by different symbols and different colors as in Fig. 6. When the reversal rate increases, on the one hand the tendency of formation of large clusters decreases, on the other hand the propensity of spiral formation in the system is progressively suppressed.

In Fig. 9, we plot the two quantities as functions of the bending stiffness, comparing different reversal rates. These results confirm the qualitative observation from the snapshots: Reversals reduce both spiral and cluster abundance, for all values of the bending stiffness. Higher reversal rates result in stronger reduction.

Having noticed this stark effect of the reversal rate on pattern formation by active filaments, we next investigate the effects of the reversal rate λ_r on the state diagram in the κ_b–f_a space. The results are shown in Fig. 10, for three nonzero values of λ_r, in comparison to the case without reversals. Already for the smallest nonzero reversal rate that we considered, $\lambda_r = 0.001$, the spiral state as well as the large-cluster state are strongly diminished. Increasing the reversal rate further, also the small-cluster regime moves towards larger bending stiffnesses and larger self-propulsion forces.

The suppression of spirals by reversals is rather straightforward. As mentioned earlier, in the absence of reversals, spirals dissolve only through collision with other filaments. Reversals add a second mechanism by the change in the polarity (head-tail direction): When the reversal occurs, self-propulsion is not directed inward, but rather outward, and thus the spiral unwinds (see Fig. 11) unless another reversal occurs before unwinding was complete. For small reversal rates $\lambda_r < f_a/\zeta L$, where a filament propagates by more than its body length between reversals, this is expected to happen. However, unwinding is faster than winding, because of the additional release of bending energy, such that also repeated reversals lead to a net unwinding.

Likewise, reversals add an additional mechanism for filaments to leave a cluster. Clustered filaments move collectively in one direction, so that any filament that reverses is likely to move out of the cluster, as shown in Fig. 12. Reversing filaments leave a cluster from its boundary as well as from the cluster interior, see also the movie in the Supplemental Material [57]. This shifts the balance between filaments joining a cluster and filaments leaving a cluster, resulting in smaller clusters. For very large reversal rates, clusters disappear entirely and the system becomes isotropic again. In this limit, the filaments do not show active directed motion any more, but rather move back and forth in a fashion similar to passive diffusion. Thus a melt state like for passive polymers is indeed expected, but the disorder results from an entirely nonequilibrium mechanism.

IV. SUMMARY AND CONCLUSIONS

In this study, we used particle-based simulations of self-propelled filaments to study their pattern formation and, specifically, the impact of direction reversal on these patterns. The simulations mimic bacterial gliding motility on surfaces and their assembly into clusters and swarms. In contrast to the well-studied spherical or rod-like self-propelled particles, we considered long and flexible filaments.

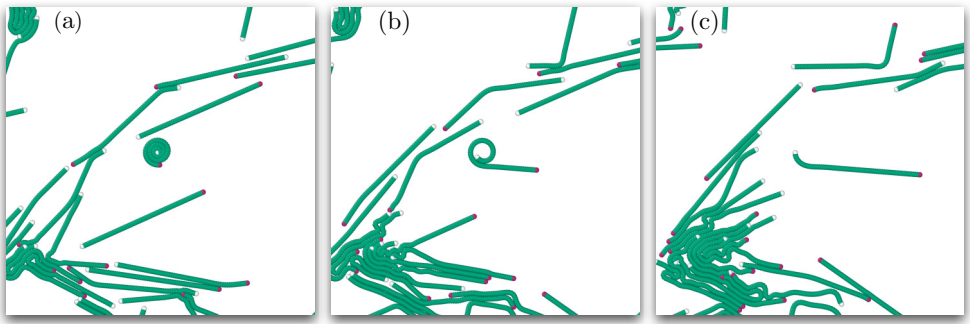

FIG. 11. Unwinding of a spiral due to the reversal dynamics. Panel (a) shows a filament in the spiral state in the center (which was formed by the collision of the tip of a filament with its own tail). In Panel (b) a reversal event takes place. Panel (c): The spiral unwinds and the filament resumes the straight configuration. The white monomer is the head of the filament, the green is the body and the purple is the tail.

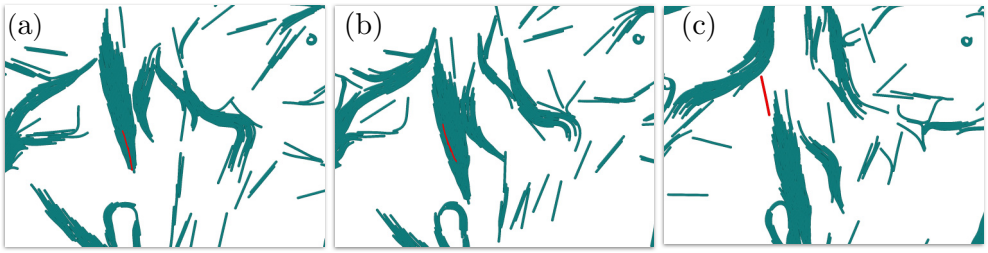

FIG. 12. Reversals allow filaments to leave a cluster: Three snapshots from a simulation that shows a large central cluster moving downwards. The filament highlighted in red reverses its direction of motion, crosses the cluster and leaves the cluster at the upper end. A movie is included in the Supplemental Material [57].

First, we discussed the patterns that could form in the absence of direction reversals, modulating the bending stiffness (κ_b) and self-propulsion force (f_a) of the filaments at a relatively low filament density. The results, in agreement with earlier studies [14,15], reflect a competition between the self-interaction of filaments, possible due to their flexibility, and the interaction between filaments. At low bending stiffness and high self-propulsion force, the self-interactions are dominant, leading to the formation of spirals. However, when the bending stiffness increases, the self-interaction is reduced and steric interactions between filaments become more important. In that case, filaments form clusters through collisions and move collectively in these clusters. Based on systematic simulations, we have determined a diagram of states in the $\kappa_b - f_a$ space.

Then, to understand the impact of stochastic direction reversals, we added a reversal rate to the filaments' dynamics, mimicking the run-reverse movement of bacteria, and examined the effects of this additional control parameter on the formation of motility patterns. In general, reversals counteract both clustering and spiral formation, thus resulting in more isotropic structures. Both negative effects can be understood via the dynamical pathways on which these structures are dissolved: In the absence of reversals, spirals are rather stable. A spirals dissolves, when a moving filament collides with it. Reversals add a second mechanism for dissolving a spirals by interrupting the spooling of spirals and inducing its unspooling. Likewise, reversals also adds new mechanisms for filaments to leave a cluster, as filaments typically leave a coherently moving cluster upon reversal. The additional mechanism for leaving clusters results in smaller clusters compared to the no-reversal reference case. Finally, high reversal rates result in purely back-and-forth motion, similar to a passive scenario.

Our results show that the direction reversals have a strong impact on the patterns of active filaments by preventing the formation of spirals and reducing clustering. For microorganisms, direction changes such as reversals are known to have a role in responses to external signals such as chemical gradients or light. Our results suggest that in addition, they have an influence on the structure of a colony. Therefore it will be interesting to study the impact of reversals in systems with higher densities.

ACKNOWLEDGMENTS

We are grateful to Rituparno Mandal for helpful discussions. This research was conducted within the Max Planck School Matter to Life, supported by the German Federal Ministry of Education and Research (BMBF) in collaboration with the Max Planck Society.

[1] M. C. Marchetti, J. F. Joanny, S. Ramaswamy, T. B. Liverpool, J. Prost, M. Rao, and R. A. Simha, Hydrodynamics of soft active matter, Rev. Mod. Phys. **85**, 1143 (2013).

[2] C. Bechinger, R. Di Leonardo, H. Löwen, C. Reichhardt, G. Volpe, and G. Volpe, Active particles in complex and crowded environments, Rev. Mod. Phys. **88**, 045006 (2016).

[3] A. A. Hyman and E. Karsenti, Morphogenetic properties of microtubules and mitotic spindle assembly, Cell **84**, 401 (1996).

[4] F. Nédélec, T. Surrey, A. C. Maggs, and S. Leibler, Self-organization of microtubules and motors, Nature (London) **389**, 305 (1997).

[5] T. Surrey, F. Nédélec, S. Leibler, and E. Karsenti, Physical properties determining self-organization of motors and microtubules, Science **292**, 1167 (2001).

[6] N. H. Mendelson, A. Bourque, K. Wilkening, K. R. Anderson, and J. C. Watkins, Organized cell swimming motions in *Bacillus subtilis* colonies: Patterns of short-lived whirls and jets, Am. Soc. Microbiol. J. **181**, 600 (1999).

[7] J. K. Parrish, S. V. Viscido, and D. Grunbaum, Self-organized fish schools: An examination of emergent properties, Biol. Bull. **202**, 296 (2002).

[8] C. Dombrowski, L. Cisneros, S. Chatkaew, R. E. Goldstein, and J. O. Kessler, Self-Concentration and Large-Scale Coherence in Bacterial Dynamics, Phys. Rev. Lett. **93**, 098103 (2004).

[9] G. Salbreux and F. Jülicher, Mechanics of active surfaces, Phys. Rev. E **96**, 032404 (2017).

[10] L. Hall-Stoodley, J. W. Costerton, and P. Stoodley, Bacterial biofilms: From the natural environment to infectious diseases, Nat. Rev. Microbiol. **2**, 95 (2004).

[11] J. M. Moore, T. N. Thompson, M. A. Glaser, and M. D. Betterton, Collective motion of driven semiflexible filaments tuned by soft repulsion and stiffness, Soft Matter **16**, 9436 (2020).

[12] A. Joshi, E. Putzig, A. Baskaran, and M. F. Hagan, The interplay between activity and filament flexibility determines the emergent properties of active nematics, Soft Matter **15**, 94 (2019).

[13] M. Bär, R. Großmann, S. Heidenreich, and F. Peruani, Self-propelled rods: Insights and perspectives for active matter, Annu. Rev. Condens. Matter Phys. **11**, 441 (2020).

[14] K. R. Prathyusha, S. Henkes, and R. Sknepnek, Dynamically generated patterns in dense suspensions of active filaments, Phys. Rev. E **97**, 022606 (2018).

[15] Ö. Duman, R. E. Isele-Holder, J. Elgeti, and G. Gompper, Collective dynamics of self-propelled semiflexible filaments, Soft Matter **14**, 4483 (2018).

[16] X. qing Shi and H. Chaté, Self-propelled rods: Linking alignment-dominated and repulsion-dominated active matter, arXiv:1807.00294.

[17] Y.-K. Wang, C.-J. Lo, and W.-C. Lo, Formation of spiral coils among self-propelled chains, Phys. Rev. E **98**, 062613 (2018).

[18] R. Großmann, F. Peruani, and M. Bär, Mesoscale pattern formation of self-propelled rods with velocity reversal, Phys. Rev. E **94**, 050602(R) (2016).

[19] S. Weitz, A. Deutsch, and F. Peruani, Self-propelled rods exhibit a phase-separated state characterized by the presence of active stresses and the ejection of polar clusters, Phys. Rev. E **92**, 012322 (2015).

[20] R. Balagam and O. A. Igoshin, Mechanism for collective cell alignment in *Myxococcus xanthus* bacteria, PLoS Comput. Biol. **11**, e1004474 (2015).

[21] R. E. Isele-Holder, J. Elgeti, and G. Gompper, Self-propelled worm-like filaments: Spontaneous spiral formation structure and dynamics, Soft Matter **11**, 7181 (2015).

[22] M. Abkenar, K. Marx, T. Auth, and G. Gompper, Collective behavior of penetrable self-propelled rods in two dimensions, Phys. Rev. E **88**, 062314 (2013).

[23] H. H. Wensink and H. Löwen, Emergent states in dense systems of active rods: From swarming to turbulence, J. Phys.: Condens. Matter **24**, 464130 (2012).

[24] H. H. Wensink and H. Löwen, Aggregation of self-propelled colloidal rods near confining walls, Phys. Rev. E **78**, 031409 (2008).

[25] L. Abbaspour and S. Klumpp, Enhanced diffusion of a tracer particle in a lattice model of a crowded active system, Phys. Rev. E **103**, 052601 (2021).

[26] U. Börner, A. Deutsch, H. Reichenbach, and M. Bär, Rippling Patterns in Aggregates of Myxobacteria Arise from Cell-Cell Collisions, Phys. Rev. Lett. **89**, 078101 (2002).

[27] Y. Sumino, K. H. Nagai, Y. Shitaka, D. Tanaka, K. Yoshikawa, H. Chaté, and K. Oiwa, Large-scale vortex lattice emerging from collectively moving microtubules, Nature (London) **483**, 448 (2012).

[28] F. Peruani, J. Starruß, V. Jakovljevic, L. Søgaard-Andersen, A. Deutsch, and M. Bär, Collective Motion and Nonequilibrium Cluster Formation in Colonies of Gliding Bacteria, Phys. Rev. Lett. **108**, 098102 (2012).

[29] A. Rabani, G. Ariel, and A. Béer, Collective motion of spherical bacteria, PLoS ONE **8**, e83760 (2013).

[30] J. Dunkel, S. Heidenreich, K. Drescher, H. H. Wensink, M. Bär, and R. E. Goldstein, Fluid Dynamics of Bacterial Turbulence, Phys. Rev. Lett. **110**, 228102 (2013).

[31] A. Béer, S. K. Strain, R. A. Hernández, E. Ben-Jacob, and E.-L. Florin, Periodic reversals in *Paenibacillus dendritiformis* swarming, J. Bacteriol. **195**, 2709 (2013).

[32] D. Nishiguchi, K. H. Nagai, H. Chaté, and M. Sano, Long-range nematic order and anomalous fluctuations in suspensions of swimming filamentous bacteria, Phys. Rev. E **95**, 020601(R) (2017).

[33] L. Huber, R. Suzuki, T. Krüger, E. Frey, and A. Bausch, Emergence of coexisting ordered states in active matter systems, Science **361**, 255 (2018).

[34] S. Nakata, V. Pimienta, I. Lagzi, H. Kitahata, and N. J. Suematsu, *Self-Organized Motion: Physicochemical Design Based on Nonlinear Dynamics*, Theoretical and Computational Chemistry Series (The Royal Society of Chemistry, 2019), pp. P001–371.

[35] T. Mirfakhrai, J. D. Madden, and R. H. Baughman, Polymer artificial muscles, Mater. Today **10**, 30 (2007).

[36] S. Nakata, K. Kayahara, M. Kuze, E. Ginder, M. Nagayama, and H. Nishimori, Synchronization of self-propelled soft pendulums, Soft Matter **14**, 3791 (2018).

[37] H. H. Wensink, J. Dunkel, S. Heidenreich, K. Drescher, R. E. Goldstein, H. Löwen, and J. M. Yeomans, Meso-scale turbulence in living fluids, Proc. Natl. Acad. Sci. USA **109**, 14308 (2012).

[38] Z. Mokhtari and A. Zippelius, Dynamics of Active Filaments in Porous Media, Phys. Rev. Lett. **123**, 028001 (2019).

[39] L. Turner, W. S. Ryu, and H. C. Berg, Real-time imaging of fluorescent flagellar filaments, J. Bacteriol. **182**, 2793 (2000).

[40] R. Großmann, F. Peruani, and M. Bär, Diffusion properties of active particles with directional reversal, New J. Phys. **18**, 043009 (2016).

[41] I. Santra, U. Basu, and S. Sabhapandit, Active Brownian motion with directional reversals, Phys. Rev. E **104**, L012601 (2021).

[42] Z. Zhang, O. A. Igoshin, C. R. Cotter, and L. J. Shimkets, Agent-based modeling reveals possible mechanisms for observed aggregation cell behaviors, Biophys. J. **115**, 2499 (2018).

[43] A. Codutti, K. Bente, D. Faivre, and S. Klumpp, Chemotaxis in external fields: Simulations for active magnetic biological matter, PLoS Comput. Biol. **15**, e1007548 (2019).

[44] K. S. Olsen, L. Angheluta, and E. G. Flekkøy, Collective states of active matter with stochastic reversals: Emergent chiral states and spontaneous current switching, Phys. Rev. Res. **4**, 043017 (2022).

[45] C. Kurzthaler, S. Mandal, T. Bhattacharjee, H. Löwen, S. S. Datta, and H. A. Stone, A geometric criterion for the optimal spreading of active polymers in porous media, Nat. Commun. **12**, 7088 (2021).

[46] M. J. McBride, Bacterial gliding motility: Multiple mechanisms for cell movement over surfaces, Annu. Rev. Microbiol. **55**, 49 (2001).

[47] C. Tamulonis, M. Postma, and J. Kaandorp, Modeling filamentous cyanobacteria reveals the advantages of long and fast trichomes for optimizing light exposure, PLoS ONE **6**, e22084 (2011).

[48] J. Taktikos, H. Stark, and V. Zaburdaev, How the motility pattern of bacteria affects their dispersal and chemotaxis, PLoS ONE **8**, e81936 (2013).

[49] D.-P. Häder and U. Burkart, Enhanced model for photophobic responses of the blue-green alga, *Phormidium uncinatum*, Plant Cell Physiol. **23**, 1391 (1982).

[50] D. Häder, Photosensory behavior in procaryotes, Microbiol. Rev. **51**, 1 (1987).

[51] H. C. Berg and D. A. Brown, Chemotaxis in *Escherichia coli* analysed by three-dimensional tracking, Nature (London) **239**, 500 (1972).

[52] Z. Alirezaeizanjani, R. Großmann, V. Pfeifer, M. Hintsche, and C. Beta, Chemotaxis strategies of bacteria with multiple run modes, Sci. Adv. **6**, eaaz6153 (2020).

[53] J. A. Anderson, J. Glaser, and S. C. Glotzer, Hoomd-blue: A python package for high-performance molecular dynamics and hard particle Monte Carlo simulations, Comput. Mater. Sci. **173**, 109363 (2020).

[54] V. Ramasubramani, B. D. Dice, E. S. Harper, M. P. Spellings, J. A. Anderson, and S. C. Glotzer, freud: A software suite for high throughput analysis of particle simulation data, Comput. Phys. Commun. **254**, 107275 (2020).

[55] K. Sekimoto, N. Mori, K. Tawada, and Y. Y. Toyoshima, Symmetry Breaking Instabilities of an *In Vitro* Biological System, Phys. Rev. Lett. **75**, 172 (1995).

[56] R. G. Winkler, J. Elgeti, and G. Gompper, Active polymers—Emergent conformational and dynamical properties: A brief review, J. Phys. Soc. Jpn. **86**, 101014 (2017).

[57] See Supplemental Material at http://link.aps.org/supplemental/10.1103/PhysRevResearch.5.013171 for a simulation movie.